Front. Chem. Sci. Eng. 2022, 16(8): 1198–1210
https://doi.org/10.1007/s11705-021-2133-z

RESEARCH ARTICLE

Sulfonic acid-functionalized mesoporous silica catalyst with different morphology for biodiesel production

Vinayak Hegde, Parimal Pandit, Pranita Rananaware, Varsha P. Brahmkhatri (✉)

Centre for Nano and Material Sciences, Jain University, Jain Global Campus, Bengaluru 562112, India

Abstract Sulfonic acid functionalized mesoporous silica based solid acid catalysts with different morphology were designed and fabricated. The synthesized materials were characterized by various physicochemical and spectroscopic techniques like scanning electron microscope-energy dispersive X-ray spectroscopy, Fourier transform infrared spectroscopy, Brunauer–Emmett–Teller surface area, thermogravimetric analysis and *n*-butylamine acidity. The shape of catalysts particles plays an important role in its activity. The sulfonic acid functionalized mesoporous silica catalysts of spherical shape and the cube shape were assessed for catalytic activity in biodiesel production. The catalytic biodiesel production reaction over the catalysts were studied by esterification of free fatty acid, oleic acid with methanol. The effect of various reaction parameters such as catalyst concentration, acid/alcohol molar ratio, catalyst amount, reaction temperature and reaction time on catalytic activity were investigated to optimize the conditions for maximum conversion. It was sulfonated cubic shape mesoporous silica which exhibited better activity as compared to the spherical shape silica catalysts. Additionally, the catalyst was regenerated and reused up to three cycles without any significant loss in activity. The present catalysts exhibit superior performance in biodiesel production and it can be used for the several biodiesel feedstock's that are rich in free fatty acids.

Keywords solid acid catalyst, mesoporous silica, sulfonic acid, biodiesel, esterification, oleic acid

1 Introduction

The conventional energy resources like coal, petroleum and natural gas are available in limited quantity in nature and they failed to accomplish constantly increasing energy demand in current times. The utilization of alternative fuels like biofuel can meet this increasing energy demand [1]. Biodiesel can be an alternative for the diesel fuels in diesel engines. Biodiesel is defined as the monoalkyl esters of long chain fatty acid derived from a renewable lipid feedstock such as vegetable oils or animal fat. It typically comprises alkyl fatty acid (chain length C_{14}–C_{22}) esters of short chain alcohols [2–4]. It can be used as a substitute of diesel fuel or it can be blended with the fuels as the combustion properties of the biodiesel are same as that of the petroleum-based diesel [5–7].

Generally biodiesel is produced by transesterification of vegetable oils or esterification of fatty acids and the process is catalyzed by either acids or bases, the conventional ones like HCl, H_2SO_4, KOH and NaOH [8,9]. Homogenous acid catalysts result in high yield of biodiesel in esterification and transesterification reaction. The conventional homogeneous catalysts suffer from corrosion, separation and environmental issues [10]. Equated to homogeneous acid catalysts, heterogenous acid catalyst shows better activity as they can eliminate the product separation procedures which eventually leads to the simplified biodiesel production and reduction in the overall process cost. Stimulated by this fact, a variety of heterogeneous acid catalysts for biodiesel production has been reported in the literature [11–15]. Among various solid acids, sulfonic acid functionalized mesoporous silica have been used in variety of acid catalyzed organic transformations [16,17]. Though, the catalytic efficiency of these catalysts still remains a great challenge in biodiesel production.

Surface functionalized mesoporous silica materials find applications in different fields like catalysis [18], environmental remediation [19], adsorption, bio-medicine [20], energy storage and in various multidisciplinary fields [21]. The surface functionalization enhances the surface activity and the adsorption capacity of the mesoporous materials. Though the inert surface of these materials results in

Received June 5, 2021; accepted October 21, 2021

E-mails: b.varsha@jainuniversity.ac.in, brahmkhatri.varsha@gmail.com

uncontrolled functionalization. There are variety of strategies to improve the surface of mesoporous materials and translate them in to new advanced materials with novel functionalities; such as immobilization, substitution grafting, surface coating, ion exchange, and organic-inorganic hybrid frameworks [11].

The literature survey shows that there are several reports on functionalization of mesostructured silica with organic surface groups [22]. In spite of promising developments, leaching of the active sites, low surface area and pore size and stability problem at higher temperature are the main drawbacks of surface functionalization of mesoporous silica. Amongst all functionalized mesoporous silica, sulfonic acid functionalized heterogeneous acid catalysts are impending as they exhibit better activity and higher efficacy [23]. This superior performance is attributed to sulfonic acid groups as they provide strong acidity and a greater number of acid sites than most of the solid acid catalysts available as reported in the recent research [24,25]. Peixoto et al. reported aryl-organosulfonic acid functionalized silica nanoparticles for esterification of free fatty acids (levulinic acid). The catalyst was synthesized by post-grafting strategy and depicted better catalytic performance in biodiesel production as compared to conventional homogenous acid catalysts [26]. Zhang et al. reported sulfonic acid functionalized tin-incorporated SBA-15 mesoporous silica catalysts of two different kinds based on synthesis methods that is one pot functionalization and the other is post functionalization. The former exhibited better catalytic activity in biodiesel production due to the better acidity [27]. Kasinathan et al. demonstrated different synthesis methods to impart hydrophobicity to solid acid catalyst, sulfonic acid functionalized silica and used for esterification of octanol with acetic acid [28]. Including biodiesel production sulfonic acid functionalized silica have been reported for various other organic reactions [16,29–32]. These reports majorly either focus on the sulfonic acid group synthesis strategies for mesoporous silica or on improving the catalytic activity. The reports on effect of textural properties of mesoporous silica such as surface area, pore size and shape on catalytic activity are very scanty [33–35].

The present work emphasizes sulfonic acid functionalized mesoporous silica catalyst of different morphology (spheres and cubes), synthesized by post synthesis modification. The catalyst synthesis was carried out in two steps, organosilylation to get thiol functionalization followed by oxidation of sulfide groups to achieve sulfonic acid functionalized mesoporous silica catalysts. The synthesized catalysts of two different surface morphology, sphere and cubes were designated as S–SOH and C–SOH respectively. All the synthesized materials and the catalysts were characterized by various physicochemical techniques. The application of these solid acid catalysts was studied in esterification of free fatty acid, oleic acid (OA) with methanol to get methyl oleate. OA comprises of more than 50% of fatty acids in animal fats. Methyl oleate is frequently used in additives, pharmaceuticals, fragrances, surfactants, cosmetics and also a useful raw material in chemical industry. There is an increasing demand of organic ester due to the rapid increase in consumption rate [4]. The core intention of the current study is to explore the effect of different shape of sulfonated mesoporous silica catalysts (S–SOH spheres and C–SOH cubes) on catalytic activity in biodiesel production and in conversion of OA. The catalytic results demonstrated that, both the catalysts were quite active but the cube shaped sulfonated mesoporous silica catalyst exhibited better activity in biodiesel production. Further the catalysts were recycled and reused.

2 Experimental

2.1 Materials

All chemicals were of analytical grade and used as received without further purification: cetyltrimethyl ammonium bromide (CTAB), tetraethyl orthosilicate (TEOS), *n*-hexane, ammonia solution, ethanol, HCl, (3-mercaptopropyl)trimethoxysilane (MPTMS), methanol, OA were obtained from Sigma Aldrich.

2.2 Synthesis of mesoporous silica with various morphology

To get the required mesoporous silica nanoparticles of different morphology, the modified Stobber's method [36] was used. The CTAB, 0.5 g was dissolved in 80 mL distilled water. The ammonia solution, 1.5 mL of (28%) was added drop wise to the CTAB solution under continuous stirring. Further, a mixture of solution of *n*-hexane (10 mL) and TEOS (2.5 mL) were added into the solution drop wise under continuous stirring. The prepared reaction mixture was kept at 35 °C at 200 $r \cdot min^{-1}$. After 12 h the solution was centrifuged and washed with ethanol water solution. The collected samples were dispersed in 1 $mol \cdot L^{-1}$ HCl (1.75 mL) and ethanol (50 mL) solution and kept at 80 °C for 8 h to remove the template in present case CTAB. Then solution is centrifuged and washed with the ethanol for 4 times and vacuum dried for 10 h. This results in spherical mesoporous silica nanoparticles detonated as SNP. Similarly for cubes, quantity of catalyst was reduced by increasing the amount of concentrated ammonia water from 1.5 to 4 mL. The obtained material was designated as CNP.

2.3 Functionalized mesoporous silica nanoparticles (S–SH and C–SH)

To get thiol functionalized silica nanoparticles, around 1 g of the prepared nanoparticles (SNP or CNP) were

dispersed in 50 mL ethanol, followed by addition of 630 μL MPTMS. The reaction mixture was left at room temperature for 24 h with continues stirring. The mesoporous silica nanoparticles with thiol group were obtained. The materials obtained were designated as S–SH and C–SH for spherical and cubic mesoporous silica nanoparticles respectively. Minor components of product were used for characterization to confirm the –SH functionalization, and remaining products were used for further process.

2.4 Synthesis of catalysts (S–SOH and C–SOH)

The thiol functionalized samples, S–SH and C–SH were further oxidized to achieve the desired catalysts. The thiol group is converted into sulfonic acid group by oxidizing the thiol group using H_2O_2 as oxidizing agent. Thiol functionalized SNP and CNP were taken around 1 g and 32 mL of 30% H_2O_2 was added. The reaction was carried out under continues stirring for 1 h at room temperature. Further, product is centrifuged and washed with distilled water and suspended in 32 mL of 10%. H_2SO_4 for 1 h to ensure the conversion of all thiol groups into sulfonic acid groups, followed by drying at 60 °C. The obtained catalysts (S–SOH and C–SOH) were characterized by various techniques. Post H_2O_2 treatment, H_2SO_4 was added to ensure the protonation of all the sulphonic acid groups. As the conventional methods of oxidation of thiols using various oxidizing agents shows some disadvantages like long reaction time, difficult workup, low yields, requirement of strong oxidizing agents, strong acidic or basic media and also in some cases use of expensive, and harmful reagents that are not environment friendly [37]. The two-step synthesis strategy for getting sulfonic acid functionalized silica is shown in Scheme 1.

2.5 Catalytic reaction

The esterification of OA (0.01 mol) with methanol (0.4 mol) and ethanol (0.4 mol) was carried out in a 100 mL batch reactor provided with a double walled air condenser, magnetic stirrer and a guard tube. The reaction mixture was refluxed at 60 °C for 6 h. The obtained products were analyzed on gas chromatograph (SHIMADZU GCMS-QP2010SE). Products were identified by comparison with the authentic samples and finally by gas chromatography-mass spectroscopy.

2.6 Characterization

The surface morphology of all the materials, SNP, S–SH, S–SOH, CNP, C–SH and C–SOH was analyzed by field emission scanning electron microscope (SEM, JEOL JSM-7100F). Adsorption–desorption isotherms of N_2 for samples were recorded on a Belsorp-Max, Microtrac BEL, Japan surface area analyzer. From adsorption-desorption isotherms surface area and pore volume were calculated based on Brunauer–Emmett–Teller (BET) equation. Powder X-ray diffraction (XRD) patterns were recorded on an Ultima IV X-ray diffractometer (Rigaku Corporation, Japan) using Ni-filtered Cu Kα radiation (l = 1.5406 Å) with a 2θ scan speed of 1.0°·min^{-1} and a 2θ scan range of 5°–80° at 40 kV and 30 Ma. X-ray photoelectron spectroscopy analysis was carried out using VG multi lab 2000; 3.125 MeV, using Al-Kα source. To confirm the surface functionalization, Fourier transform infrared (FTIR) spectra of all the materials were recorded using KBr pellet on Bruker FTIR Spectrometer ALPHA-E. Thermogravimetric analysis (TGA) was carried out on Pekin Elmer Model STA 8000 instrument using N_2 as purge gas.

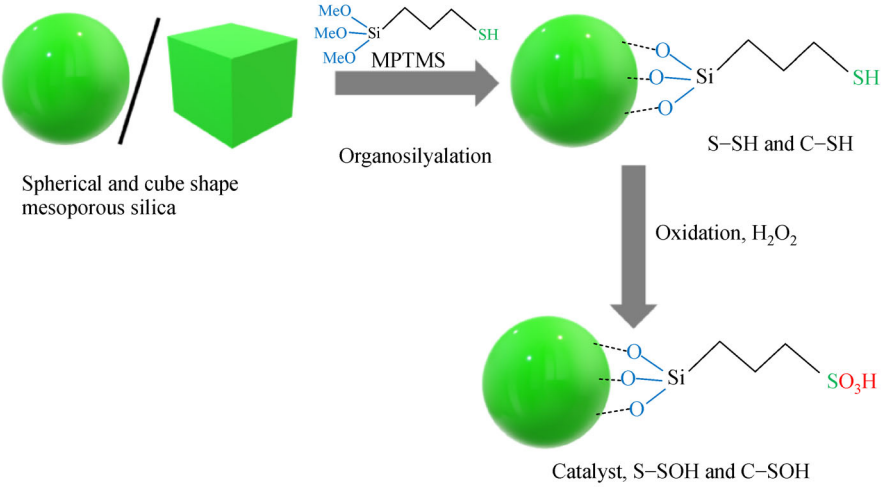

Scheme 1 Synthesis of sulfonic acid functionalized mesoporous silica.

2.7 *n*-Butylamine acidity measurement

The total acidity for all the materials, SNP, S–SOH, CNP and C–SOH was determined by *n*-butylamine titration [14]. A solution of *n*-butylamine (0.025 mol·L^{-1}) in toluene was used for acidity measurements. The catalyst weighing 0.5 g was suspended in *n*-butylamine (0.025 mol·L^{-1}) solution for 24 h. After 24 h samples were centrifuged and the excess base in the solution was titrated against trichloroacetic acid in toluene using neutral red as an indicator. This gives the total acidity of the materials.

3 Results and discussion

3.1 Characterization of mesoporous silica nanoparticles with various morphology (SNP and CNP)

The synthesized SNP and CNP materials were characterized by various spectroscopic techniques. Only the main characterization techniques such as XRD, SEM, and BET surface area measurements are presented here and the rest of the techniques will be discussed along with the catalyst characterization in subsequent sections. Figure 1 shows the SEM images of SNP and CNP. The SEM images showed the uniform growth of spherical morphology (Figs. 1(a–c)) and cube shape particle morphology (Figs. 1(d–f)) in case of SNP and CNP respectively. The SNP showed uniform spherical particles of 100–150 nm. Whereas in case of CNP, uniform cubes of around 300–400 nm size were observed. The CNP sample exhibited poly dispersed cubes with clear edges and corners and six equivalent {100} planes, indicating a well-faceted single crystal morphology (Fig. 1(f)).

The XRD patterns of SNP and CNP are shown in Fig. S1 (cf. Electronic Supplementary Material, ESM). The XRD patterns of the mesoporous silica nanoparticles indicate a broad peak at $2\theta = 22°$, which reveals the amorphous nature of the mesoporous silica materials. The surface area of SNP and CNP was found to be 1078 and 1044 m$^2\cdot$g^{-1} with 6.26 and 4 nm pore diameter respectively from N_2 adsorption–desorption isotherms and will be explained in detail in forthcoming sections.

3.2 Characterization of functionalized mesoporous silica nanoparticles and catalysts

The synthesized functionalized mesoporous silica nanoparticle (S–SH and C–SH) and the catalysts (S–SOH and C–SOH) were characterized by various spectroscopic techniques such as elemental analysis, FTIR, BET surface area, XRD, SEM and TGA. The Fig. 2 shows elemental analysis of all the materials SNP, S–SH, S–SOH (Fig. 2(a)), CNP, C–SH and C–SOH (Fig. 2(b)).

The energy dispersive analysis of X-rays (EDAX) for all the materials is depicted in Table 1. SNP and CNP showed 59% and 58.85% oxygen content and 41% and 41.18% of silica content respectively. Further EDAX analysis shows presence of sulfur in S–SH, C–SH, S–SOH and C–SOH that indicates the thiol functionalization in S–SH, C–SH samples and presence of sulfonic acid group in S–SOH, C–SOH. The decrease in oxygen amount in S–SH, S–SOH, C–SH and C–SOH samples as shown in Table 1 confirmed the presence of sulfur in the materials. S–SOH and C–SOH shows more oxygen content than S–SH and C–SH respectively which is attributed to increased oxygen content upon oxidation. This eventually explains the decrease in sulfur content in S–SOH and C–SOH as compared to S–SH and C–SH.

FTIR spectra of all the materials CTAB–SNP, SNP, S–SH, S–SOH, CTAB–CNP, CNP, C–SH and C–SOH are depicted in Fig. 3. The FTIR spectra of as made silica spheres and cubes before surfactant removal, i.e., CTAB–SNP and CTAB–CNP are shown in Figs. 3(a) and 3(b) respectively, wherein the bands shown in the region 2800–3000 cm^{-1} can be attributed to the vibrations of C–H bond from CTAB surfactant templates. After ethanol extraction in all the samples, no adsorption peaks were observed in

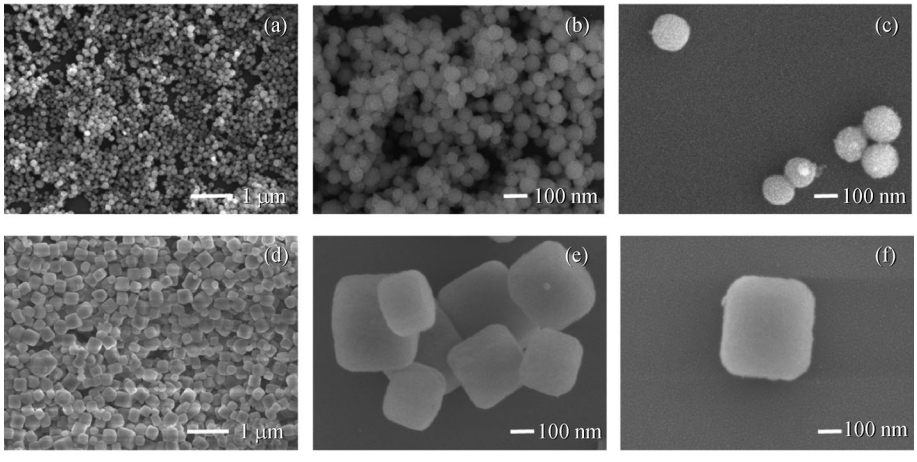

Fig. 1 SEM images of (a, b, c) SNP and (d, e, f) CNP.

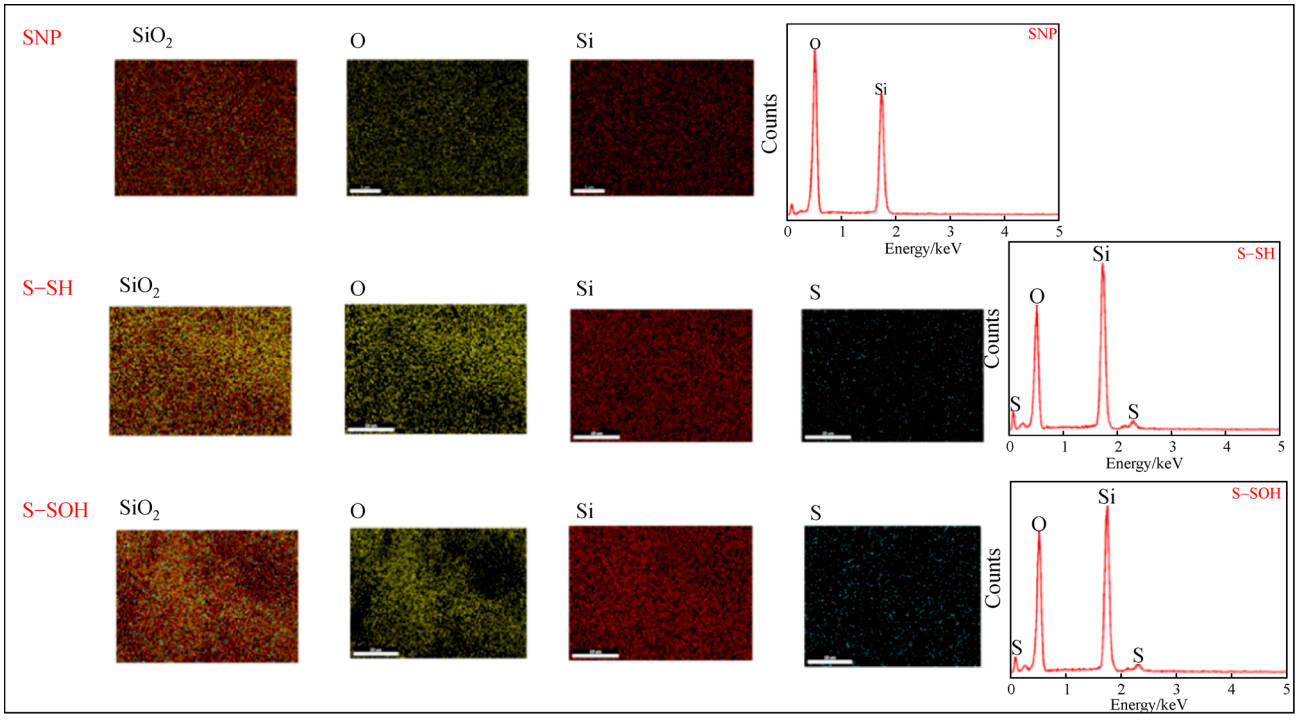

(a)

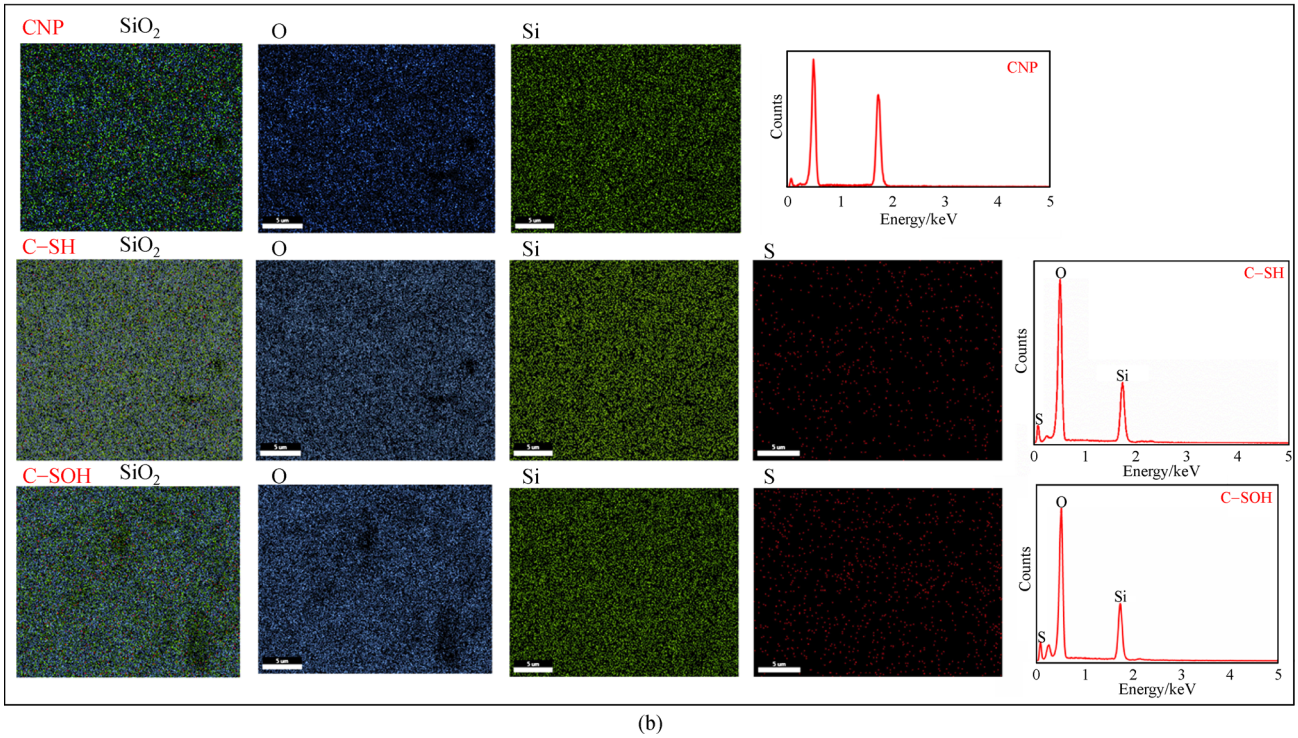

(b)

Fig. 2 (a) Elemental mapping of SNP, S–SH and S–SOH; (b) elemental mapping of CNP, C–SH and C–SOH.

the range of 2800–3000 cm^{-1}, suggesting that the CTAB template have been completely removed. The FTIR spectra of SNP and CNP both exhibited a band at 800 cm^{-1} for Si–O–Si symmetric vibration and large band between 1000 and 1250 cm^{-1} is for Si–O–Si asymmetric vibration. The broad absorption band around 3448 cm^{-1} is the absorption of Si–OH on surface, which is almost common in all samples, which provides opportunities for functionalization in silica. The weak band around 2550 to 2600 cm^{-1} was observed in S–SH and C–SH materials is attributed to thiol groups. This confirms the functionalization after organosilylation using MPTMS. Besides, after the

Table 1 Elemental analysis

Material	O/%	Si/%	S/%
SNP	59.00	41.00	–
S–SH	44.77	51.21	4.02
S–SOH	47.93	50.53	1.54
CNP	58.85	41.18	–
C–SH	64.55	30.41	5.04
C–SOH	67.43	30.22	2.35

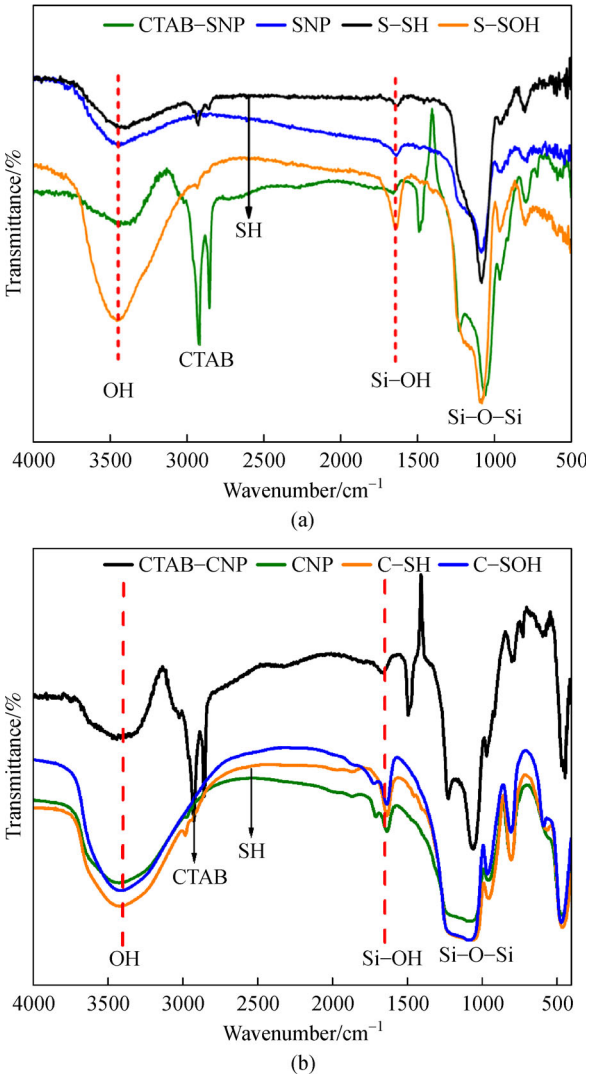

Fig. 3 (a) FTIR spectra of CTAB–SNP, SNP, S–SH and S–SOH; (b) FTIR spectra of CTAB–CNP, CNP, C–SH and C–SOH.

oxidation of thiol groups the peak at 1300 to 1350 cm^{-1} for $-SO_3H$ group is obtained in case of S–SOH and C–SOH (Figs. 3(a) and 3(b)). Hence the FTIR spectra confirms the sulfonic acid group functionalization in S–SOH and C–SOH. The observed results are in agreement with reported results earlier [28].

The N_2 adsorption-desorption isotherms of all the materials, SNP, S–SH, S–SOH, CNP, C–SH and C–SOH are shown in Fig. 4. All samples showed type of IV, N_2 adsorption-desorption isotherms (Figs. 4(a) and 4(c)) according to the IUPAC classification and exhibited an H1 hysteresis loop which is a characteristic of mesoporous silica nanoparticles [38]. The adsorption branch of each isotherm showed a sharp inflection, which means a typical capillary condensation within uniform pores and considerable adsorption amounts indicate that, there is considerable volume of nanospaces even after the functionalization. In addition, narrow pore size distribution was observed for all the materials which indicates long range order over large scales (Figs. 4(b) and 4(d)). The decrease in pore diameter in case of S–SH as compared to SNP is due to the functionalization. The similar was the case for C–SH and C–SOH samples, which is also attributed to surface functionalization.

The textural properties like surface area and pore diameter for all the materials are presented in Table 2. After the functionalization with thiol group, the decrease in surface area and pore diameter was observed for S–SH and C–SH samples. Interestingly in second step of functionalization where the –SH group was oxidized to get S–SOH and C–SOH catalysts, the surface area and pore diameter increases due to exfoliation of the structure and increase in the oxygen content post functionalization [39,40]. *n*-Butyl amine acidity values for SNP, CNP, S–SOH and C–SOH are shown in Table 2. *n*-Butyl amine acidity values of S–SOH and C–SOH with spherical and cubic morphology catalyst was observed to be higher than the bare silica materials (SNP and CNP) as expected due to the presence of sulfonic acid groups.

The SEM images of all the materials SNP, S–SH, S–SOH, CNP, C–SH, C–SOH are shown in Fig. 5. The SEM images of SNP showed uniform spherical morphology and discrete particles of 150–200 nm (Fig. 5(a)). The spherical morphology was retained post functionalization with thiol groups in case of S–SH sample and $-SO_3H$ in case of S–SOH sample respectively (Figs. 5(b) and 5(c)). There were no structural changes or formation of aggregates post functionalization in S–SH and S–SOH. The SEM images of CNP, C–SH and C–SOH are shown in Figs. 5(d–f). The SEM images reveals that the CNP consists of nanocubes of 300–400 nm (Fig. 5(d)). The nanocubes have clear edges and corners and six equivalent {100} planes, exhibiting a well faceted single crystal morphology (Fig. 5(d)) though the particle were polydisperse. After functionalization no morphological changes were observed in both S–SOH and C–SOH catalysts (Figs. 5(c) and 5(f)).

The TGA-differential analysis (DTA) curves of bare silica spheres and cubes and the –SH and $-SO_3H$ functionalized silica is depicted in Fig. 6. The bare silica spheres, SNP (Fig. 6(a)) and bare silica cubes, CNP (Fig. 6(b)) show weight loss of 8% and 10% respectively at 50 to 130 °C due to adsorbed water molecules. 3.37% and 7.11%

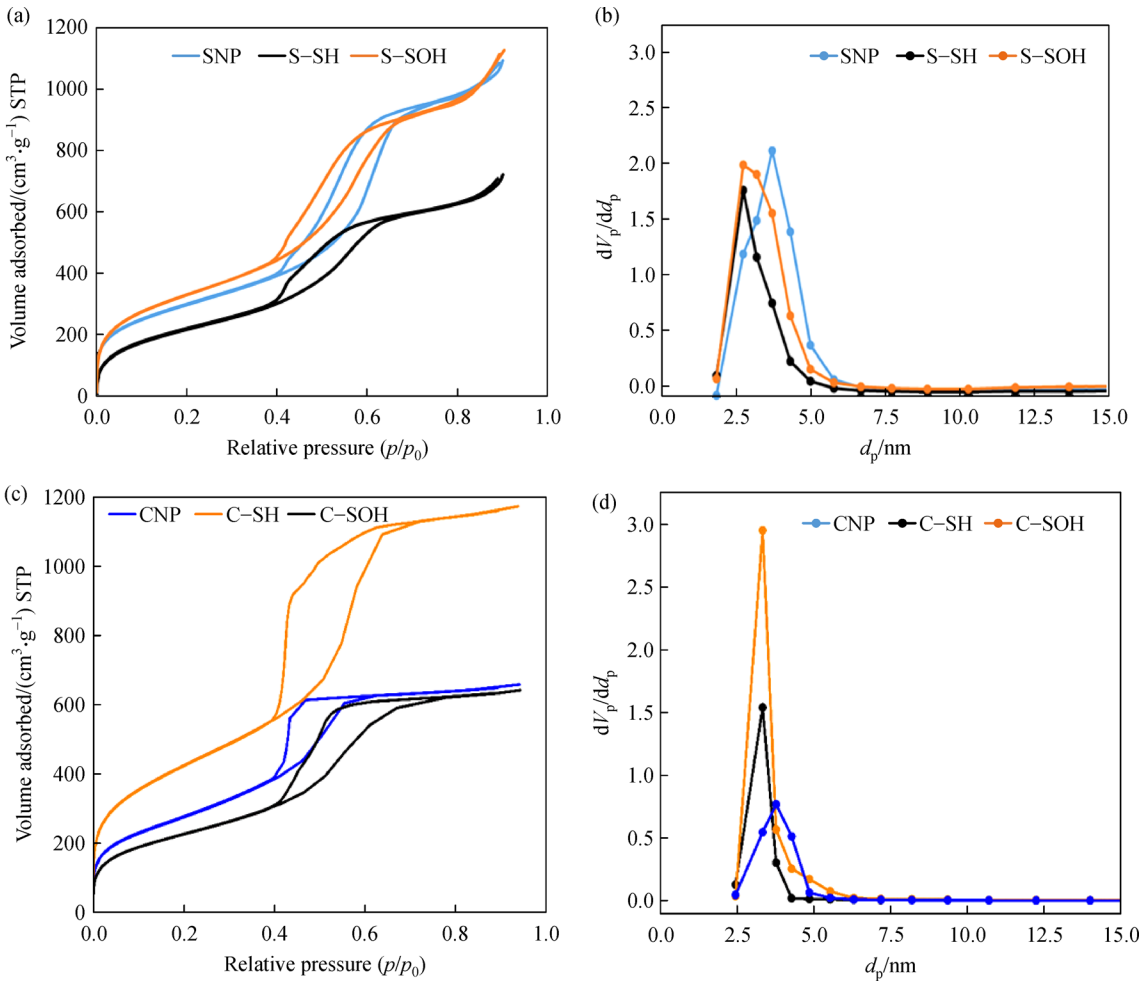

Fig. 4 (a, b) N_2 adsorption–desorption isotherms of SNP, S–SH and S–SOH; (c, d) N_2 adsorption–desorption isotherms of CNP, C–SH and C–SOH.

Table 2 Textural properties and total acidity of materials

Material	Surface area /(m^2·g^{-1})	Pore diameter /nm	*n*-Butyl amine acidity /(mmol·g^{-1})
SNP	1078	6.26	0.21
S–SH	808	5.51	–
S–SOH	1204	5.78	1.13
CNP	1044	4.00	0.48
C–SH	831	3.78	–
C–SOH	1464	4.95	1.55

weight loss corresponding to –SH group was observed at 150 to 350 °C in C–SH and S–SH materials respectively (Figs. 6(a) and 6(b)). Sulphonic group degradation was observed with 2.32% and 10.66% weight loss at 200 to 300 °C in C–SOH and S–SOH respectively. All the materials were stable up to 600 °C as observed in TGA curves as shown in Fig. 6. In general, post sulfonic acid group functionalization, the catalysts S–SOH and C–SOH were found to be most stable as compared to thiol functionalized samples. From TGA–DTA curves and the weight loss we have calculated the amount of linker (–SH) to silica ratio in S–SH and C–SH materials which was found to be 1:5 and 1:6.6 respectively. Similarly, after sulfonic acid functionalization amount of linker (–SO_3H) to silica ratio in S–SOH and C–SOH was found to be 1:3.4 and 1:4.5 respectively.

3.3 Esterification of free fatty acid

Generally, esterification of organic acids is an equilibrium-limited reaction. In order to overcome the equilibrium limitation, esterification reaction of OA is carried out by taking alcohol redundant, in present case methanol in excess in order to favor the forward reaction. The effect of various reaction parameters like acid/alcohol molar ratio, amount of catalyst, reaction time and temperature were studied to optimize the conditions for maximum conversion. The effect of mole ratio and amount of catalyst is shown in Fig. 7. To investigate the effect of mole ratio of reactants in biodiesel production, esterification reaction

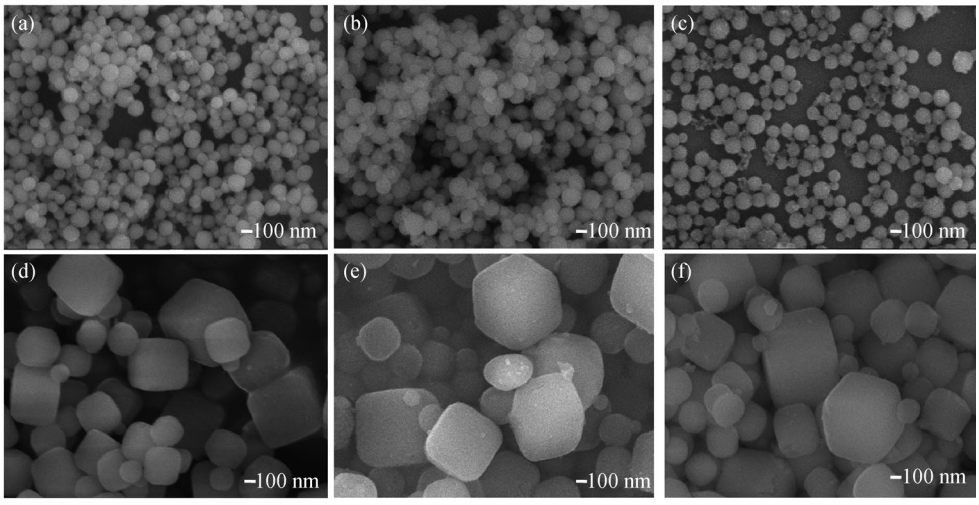

Fig. 5 SEM images of (a) SNP, (b) S–SH, (c) S–SOH, (d) CNP, (e) C–SH and (f) C–SOH.

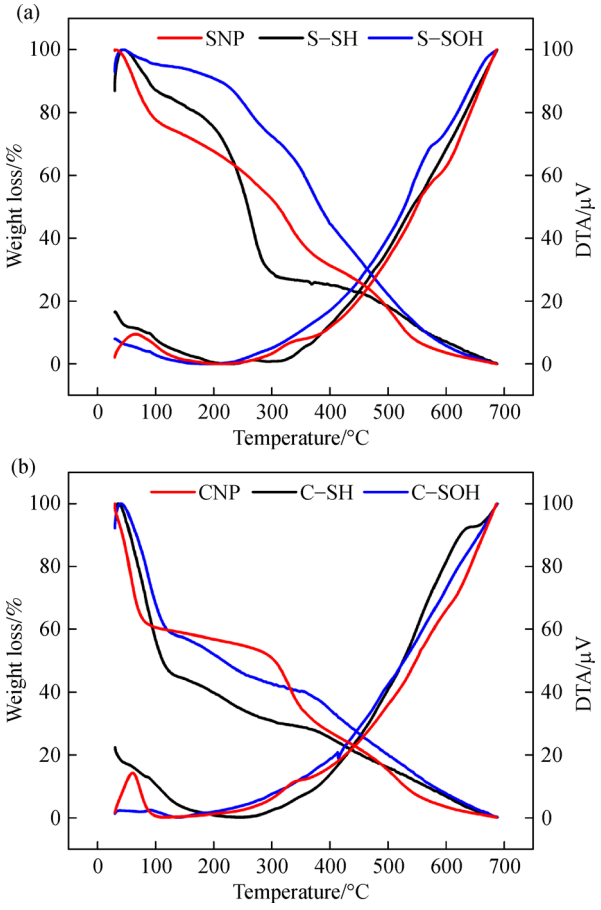

Fig. 6 TGA and DTA analysis of (a) SNP, S–SH, S–SOH and (b) CNP, C–SH, C–SOH. The data were normalized for comparison.

was carried out by varying mole ratio of OA to methanol, with 0.1 g of the catalyst for 4 h at 60 °C over both catalysts, S–SOH and C–SOH. It can be observed from Fig. 7(a) that the OA conversion increases with increase in the acid to methanol ratio and reaches to maximum conversion with the mole ratio of 1:40. With further increase in molar ratio there was only a minor increase in conversion. Hence molar ratio of 1:40 was optimized for obtaining high conversion products. The catalyst with spherical morphology, S–SOH exhibited 54% conversion and the catalyst with cubes morphology showed 62% conversion of OA.

Effect of amount of catalyst on OA conversion was investigated for both the catalysts. The catalyst amount was varied in the range of 25–100 mg. As shown in Fig. 7(b), the conversion increased with the increase in amount of catalysts (S–SOH and C–SOH) and reaches to a maximum conversion with 75 mg of catalyst. But with further increase in amount of catalyst the OA conversion remains constant. Hence 75 mg of catalyst amount was optimized. The catalyst with spherical morphology, S–SOH exhibited 60% conversion and the catalyst with cubes morphology showed 86% conversion of OA.

Effect of reaction time and temperature on conversion of fatty acids was investigated as shown in Fig. 8. It was observed from Fig. 8(a) that the OA conversion increases with increase in reaction time for both the catalysts. The OA conversion was 78% over S–SOH and 92% over C–SOH in eight hours respectively. Effect of reaction temperature on OA conversion was studied and it was found that with increase in reaction temperature conversion increases from 40 to 60 °C as depicted in Fig. 8(b). At higher temperatures like 80 °C, conversions decrease which is above the boiling point of methanol. However, the lower temperature, i.e., 60 °C was selected. Therefore, all the reactions were studied at lower temperature, i.e., 60 °C.

The optimized conditions for esterification of OA are: mole ratio of acid to alcohol 1:40; amount of catalyst 75 mg; reaction temperature 60 °C and reaction time 8 h

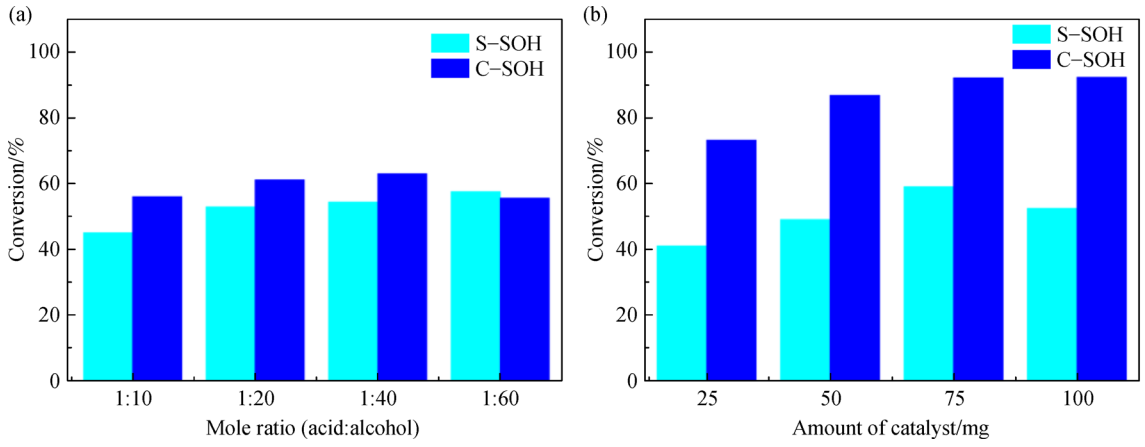

Fig. 7 (a) Effect of mole ratio acid/alcohol (reaction conditions: amount of catalyst 0.1 g; reaction temperature 60 °C; reaction time 4 h). (b) Effect of amount of catalyst (reaction conditions: mole ratio1:40; reaction temperature 60 °C; reaction time 4 h).

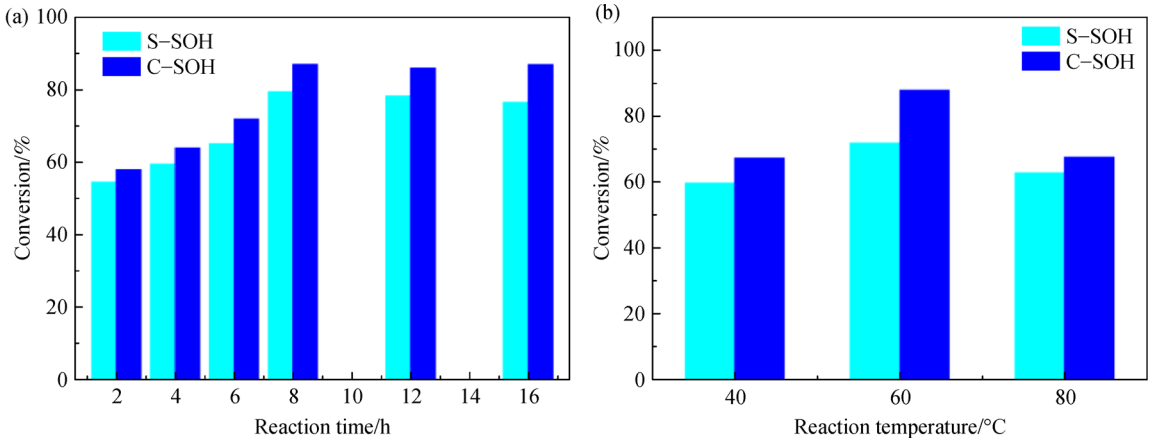

Fig. 8 (a) Effect of reaction time (reaction conditions: mole ratio of acid to alcohol 1:40; amount of catalyst 75 mg; reaction temperature 60 °C). (b) Effect of reaction temperature (reaction conditions: mole ratio of acid to alcohol 1:40; amount of catalyst 75 mg; reaction time 8 h).

over S–SOH and C–SOH. The OA esterification was also carried out with ethanol in optimized conditions and the results are presented in Fig. 9. The conversion of OA was comparatively less with ethanol as with methanol over both the catalysts, S–SOH and C–SOH, which may be due to increased chain length that may hinder the molecules towards reaching the catalytic active sites inside the mesoporous catalysts.

The catalytic activity results for OA esterification towards biodiesel production strongly depict the superior activity of C–SOH catalyst. This superior catalytic performance can be explained based on the following facts. 1) Particle size. It is well documented that smaller particles exhibit higher catalytic activity than the larger ones [41]. The difference in catalytic activity in spherical catalyst S–SOH and cubic morphology catalyst C–SOH is majorly due to the shape effect and not the size as spherical silica nano catalysts are 100–150 nm in size whereas in cubic silica nano catalyst, particle size is 300–400 nm as

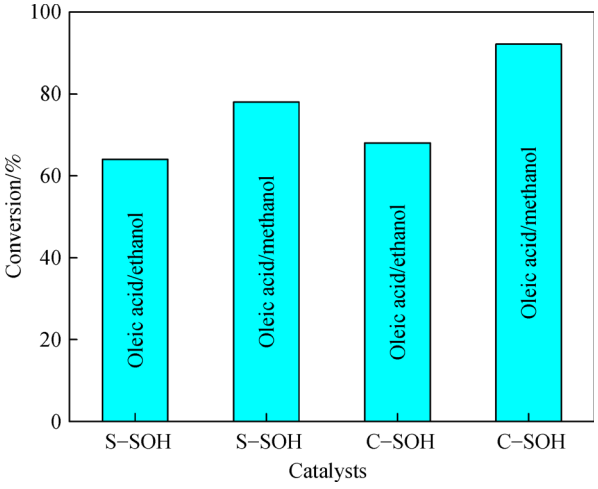

Fig. 9 Esterification of OA with methanol and ethanol in optimized conditions (reaction conditions: mole ratio of acid to alcohol 1:40; amount of catalyst 75 mg; temperature 60 °C; reaction time 8 h).

shown in SEM images in Fig. 5. Despite of larger particle size cubic silica catalyst C–SOH exhibited better activity which is due to shape effect. 2) Surface area and acidity. The higher catalytic activity of present catalysts C–SOH and S–SOH is attributed to higher functionalization of sulfonic acid groups on silica surface, higher total acidity values and higher surface area as shown in Table 2. The superior catalytic activity of C–SOH with cubic morphology is due high total acidity and surface area as compared to the S–SOH, with spherical morphology. 3) Extent of functionalization. As observed from TGA results the extent of functionalization was more in cubic silica materials C–SH and C–SOH as compared to spherical silica materials S–SH and S–SOH. As the sulfonic acid group functionalization is more, the linker to silica ratio is 1:4.5 in C–SOH catalysts, which is more than that of 1:3.4 in S–SOH catalyst. Therefore, cubic shape C–SOH exhibits better catalytic activity than spherical S–SOH catalyst in OA esterification. 4) Comparison of catalytic activity by keeping same acidity. By keeping the same acidity and by changing the amount of catalysts we can compare the shape of the catalysts for S–SOH and C–SOH. So, for S–SOH for 75 mg the *n*-butyl amine acidity will be 0.085 mmol·g^{-1}. For the same acidity value of C–SOH, the amount of catalyst required will 55 mg. Hence, for S–SOH for 75 mg, the OA conversion was found to be 78% whereas for C–SOH for 55 mg, OA conversion was found to be 82%. This difference in the catalytic activity can be attributed to the cubic shape of the catalyst.

3.4 Recycling of catalysts: catalytic activity and characterization of regenerated catalyst

The catalyst was recycled in order to test its activity as well as stability as presented in Fig. 10. The catalyst was separated from the reaction mixture only by simple filtration, first washing was given with methanol to remove unreacted OA and then the subsequent washings were done by distilled water followed by drying at 100 °C and the recovered catalyst (S–SOH–R3 and C–SOH–R3) was reused again for the further fresh reaction. To check sustainability of the synthesized catalyst, the catalytic activity of recycled catalyst after various cycles were evaluated. Also, the recycled catalysts were characterized by FTIR analysis for functional groups and for surface morphology analysis by SEM. As shown in Fig. 10(a), the

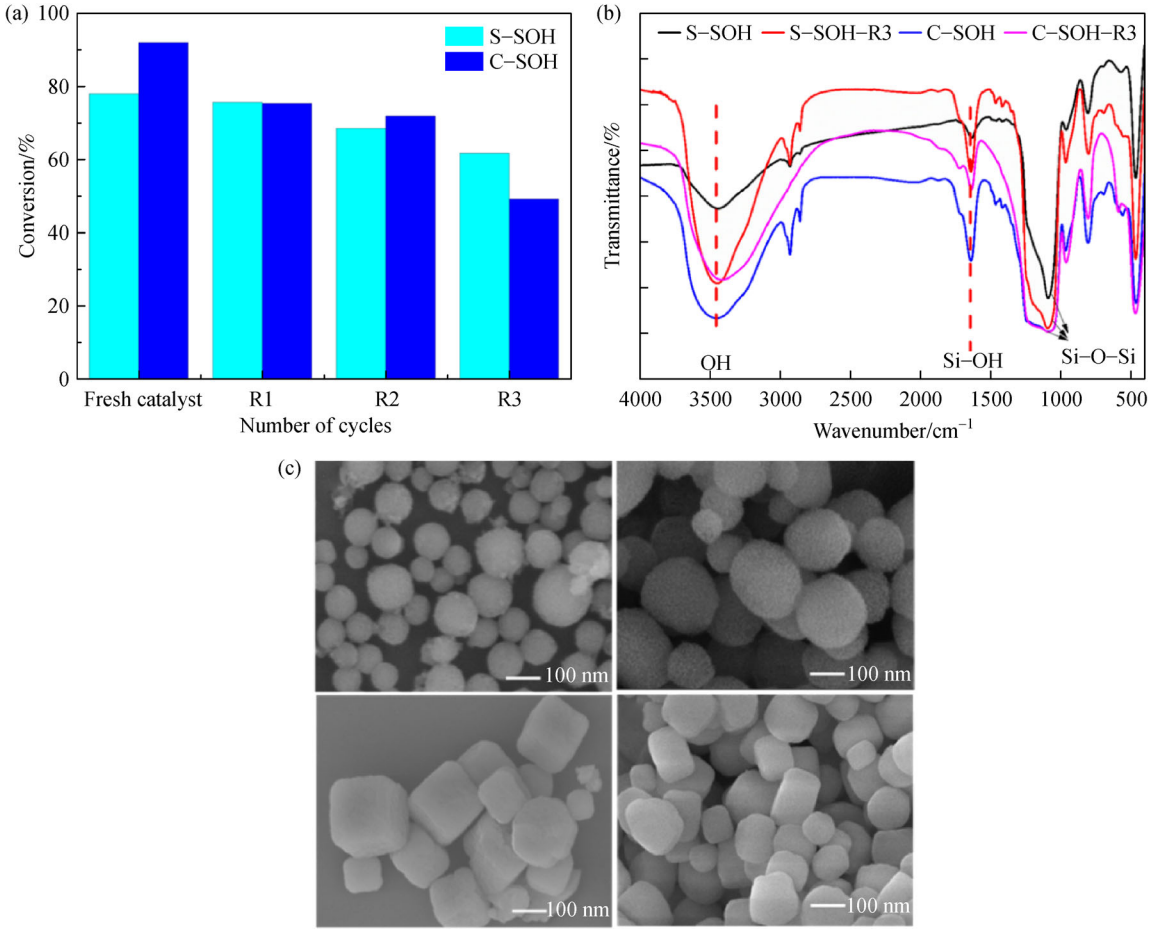

Fig. 10 Catalytic activity and characterization of recycled catalyst: (a) catalytic activity of recycled catalysts; (b) FTIR of fresh and recycled catalyst S–SOH–R3 and C–SOH–R3; (c) SEM images of fresh and recycled catalyst S–SOH–R3 and C–SOH–R3.

catalytic activity of recycled catalyst is almost the same as fresh catalyst up to two cycles. But after third cycle there was slight decrease in catalytic activity of both the catalysts S–SOH–R3 and C–SOH–R3. Hence the catalysts after third recycle S–SOH–R3 and C–SOH–R3 were characterized for FTIR and SEM analysis. The FTIR spectra (Fig. 10(b)) of regenerated catalyst shows the presence of all the characteristic bands with nearly same frequencies. The SEM images of recycled catalyst are shown in Fig. 10(c). The original spherical shape and size of the catalysts (S–SOH–R3) were retained even after three recycles. Likewise in case of C–SOH, the original cubic morphology of the catalysts was retained even after recycling (C–SOH–R3).

3.5 Comparison of OA conversion with the reported catalysts

The superiority of the present catalysts, S–SOH and C–SOH, lies in better conversion of OA under mild reaction conditions. Due to the various advantages of sulfonated mesoporous silica materials, S–SOH and C–SOH, are the potential catalysts for biodiesel production (Scheme 2).

The efficiency of present catalysts in biodiesel production was compared with the other reported sulfonic acid catalysts and presented in Table 3. It is observed from the Table 3 that 92% and 78% conversion was obtained with present catalysts, C–SOH and S–SOH respectively. The other reported catalysts based on sulfonated metal organic frameworks, sulfonated carbon and sulfonated zirconia exhibit high conversion of OA but the reaction conditions are harsh such as high temperature, high amount of catalyst used and long reaction hours as detailed in Table 3. Hence present catalysts are promising for biodiesel production by esterification of OA under mild reactions conditions, a sustainable way to produce biodiesel.

4 Conclusions

Sulfonic acid functionalized mesostructured silica with different morphology, nanosphere and cubes were successfully synthesized via two step post functionalization method. The synthesized catalysts (S–SOH and C–SOH)

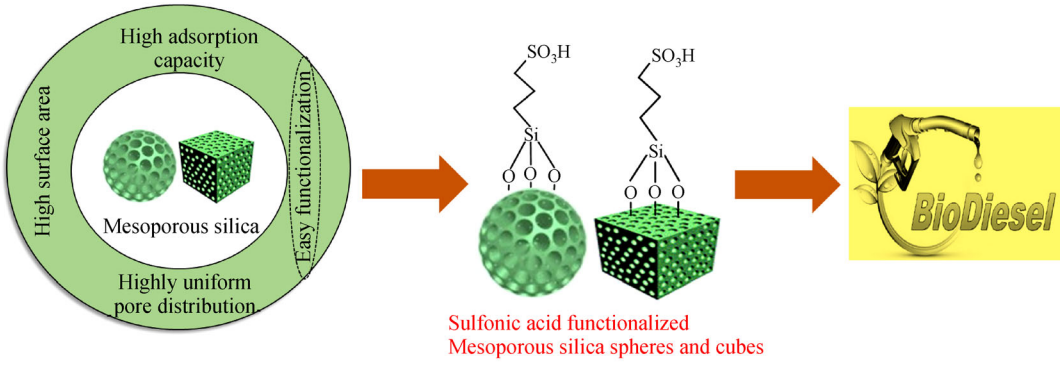

Scheme 2 Biodiesel production over sulfonated mesoporous silica (S–SNP, C–SNP).

Table 3 Production of biodiesel by esterification using different sulfonic acid-functionalized solid acid catalysts

Material	Substrate	Amount of catalyst	Mole ratio alcohol/acid	Reaction time	Reaction temperature/°C	Conversion/%	Ref.
C–SOH	OA	75 mg	40:1	8 h	60	92	Present work
S–SOH	OA	75 mg	40:1	8 h	60	78	Present work
MIL–101(Cr)–SO_3H	OA	0.1 g	10 mL methanol, 1 mL OA	20 min	120	93	[42]
Coal-based solid acid	OA	8%	Methanol: oleic acid 10:1	4 h	67	97	[43]
ICS–SO_3H	Palm fatty acid distillate	2%	Methanol:palm fatty acid distillate 10:1	3 h	75	94	[44]
Sulfonated activated carbon	OA	12%	Ethanol:OA 7:1	3 h	85	96	[45]
SO_3H@ZrP	OA	5%	Methanol:oleic acid 9:1	5 h	65	89	[46]
HSiW/SBA-15	OA	0.40 g	Methanol:OA 20:1	8 h	60	89.7	[47]
ZS/HMS	Citric acid	0.31	Citric acid (0.05 mol), *n*-butanol (0.2 mol)	2 h	120	93	[48]

were investigated for biodiesel synthesis from free fatty acid, OA. The various reaction parameters were optimized to get optimum conversion and under mild reaction conditions. C–SOH catalyst with nano cube morphology exhibited 92% conversion. This excellent catalytic performance is mainly attributed to the large surface area and pore diameter of the mesoporous silica and the Bronsted acid strength of sulfonated groups as active sites in S–SOH and C–SOH catalysts. The C–SOH with nanocubes exhibited superior activity which is attributed to high degree of sulfonic acid group functionalization, higher value of total acidity, large surface areas and large pores that facilitates the rapid transport of reactants and products through channels in mesopores. The superior activity of cubic shape sulfonic acid functionalized mesoporous silica as compared to spherical shape suggests that the catalyst morphology plays an important role in catalytic performance of the material. Moreover, both the catalysts were recycled and regenerated after simple steps without any substantial loss in activity. Mutually, the catalysts have potential to be used as superior catalyst for the biodiesel feedstocks with high free fatty acid content.

Acknowledgements We are thankful to Jain University, Bangalore, India, for providing facilities. Varsha P. Brahmkhatri also acknowledges TARE-SERB.TAR/2018/000547. Nanomission project "SR/NM/NS-20/2014" CNMS, JAIN deemed to be University is acknowledged for SEM facility.

Electronic Supplementary Material Supplementary material is available in the online version of this article at https://dx.doi.org/10.1007/s11705-021-2133-z and is accessible for authorized users.

References

1. Yang S, Yang Y, Kankala R K, Li B. Sustainability assessment of synfuels from biomass or coal: an insight on the economic and ecological burdens. Renewable Energy, 2018, 118: 870–878
2. Demirbas A. Importance of biodiesel as transportation fuel. Energy Policy, 2007, 35(9): 4661–4670
3. Demirbas A. Progress and recent trends in biodiesel fuels. Energy Conversion and Management, 2009, 50(1): 14–34
4. Chen B, Wang J, He T, Jie F, Chen B. Impact of biodiesel on engine oil quality: role of methyl oleate and performance of sulfonate detergent additive. Fuel, 2019, 244: 454–460
5. Navaneeth P V, Suraj C K, Mehta P S, Anand K. Predicting the effect of biodiesel composition on the performance and emission of a compression ignition engine using a phenomenological model. Fuel, 2021, 293: 120453
6. Jothiramalingam R, Wang M K. Review of recent developments in solid acid, base, and enzyme catalysts (heterogeneous) for biodiesel production via transesterification. Industrial & Engineering Chemistry Research, 2009, 48(13): 6162–6172
7. Kondaiah A, Sesha Rao Y, Satishkumar, Kamitkar N D, Jafar Ali Ibrahim S, Chandradass J, Kannan T T M. Influence of blends of castor seed biodiesel and diesel on engine characteristics. Materials Today: Proceedings, 2021, 45: 7043–7049
8. Macario A, Giordano G, Onida B, Cocina D, Tagarelli A, Giuffrè A M. Biodiesel production process by homogeneous/heterogeneous catalytic system using an acid-base catalyst. Applied Catalysis A, General, 2010, 378(2): 160–168
9. Guo F, Peng Z G, Dai J Y, Xiu Z L. Calcined sodium silicate as solid base catalyst for biodiesel production. Fuel Processing Technology, 2010, 91(3): 322–328
10. Boon-anuwat N, Kiatkittipong W, Aiouache F, Assabumrungrat S. Process design of continuous biodiesel production by reactive distillation: comparison between homogeneous and heterogeneous catalysts. Chemical Engineering and Processing, 2015, 92: 33–44
11. Soltani S, Rashid U, Al-Resayes S I, Nehdi I A. Recent progress in synthesis and surface functionalization of mesoporous acidic heterogeneous catalysts for esterification of free fatty acid feedstocks: a review. Energy Conversion and Management, 2017, 141: 183–205
12. Tan X, Sudarsanam P, Tan J, Wang A, Zhang H, Li H, Yang S. Sulfonic acid-functionalized heterogeneous catalytic materials for efficient biodiesel production: a review. Journal of Environmental Chemical Engineering, 2021, 9(1): 104719
13. Patel A, Brahmkhatri V, Singh N. Biodiesel production by esterification of free fatty acid over sulfated zirconia. Renewable Energy, 2013, 51: 227–233
14. Brahmkhatri V, Patel A. 12-Tungstophosphoric acid anchored to SBA-15: an efficient, environmentally benign reusable catalysts for biodiesel production by esterification of free fatty acids. Applied Catalysis A, General, 2011, 403(1): 161–172
15. Brahmkhatri V, Patel A. Biodiesel production by esterification of free fatty acids over 12-tungstophosphoric acid anchored to MCM-41. Industrial & Engineering Chemistry Research, 2011, 50(11): 6620–6628
16. Mohammadi Ziarani G, Lashgari N, Badiei A. Sulfonic acid-functionalized mesoporous silica (SBA-Pr-SO_3H) as solid acid catalyst in organic reactions. Journal of Molecular Catalysis A Chemical, 2015, 397: 166–191
17. Wang P, Zhao Y, Liu J. Versatile design and synthesis of mesoporous sulfonic acid catalysts. Science Bulletin, 2018, 63(4): 252–266
18. Verma P, Kuwahara Y, Mori K, Raja R, Yamashita H. Functionalized mesoporous SBA-15 silica: recent trends and catalytic applications. Nanoscale, 2020, 12(21): 11333–11363
19. Costa J A S, de Jesus R A, Santos D O, Neris J B, Figueiredo R T, Paranhos C M. Synthesis, functionalization, and environmental application of silica-based mesoporous materials of the M41S and SBA-*n* families: a review. Journal of Environmental Chemical Engineering, 2021, 9(3): 105259
20. Hoang Thi T T, Cao V D, Nguyen T N Q, Hoang D T, Ngo V C, Nguyen D H. Functionalized mesoporous silica nanoparticles and biomedical applications. Materials Science and Engineering C, 2019, 99: 631–656
21. Kholafazad Kordasht H, Pazhuhi M, Pashazadeh-Panahi P, Hasanzadeh M, Shadjou N. Multifunctional aptasensors based on mesoporous silica nanoparticles as an efficient platform for bioanalytical applications: recent advances. Trends in Analytical Chemistry, 2020, 124: 115778
22. Gañán J, Morante-Zarcero S, Pérez-Quintanilla D, Sierra I.

2-Mercaptopyrimidine-functionalized mesostructured silicas to develop electrochemical sensors for a rapid control of scopolamine in tea and herbal tea infusions. Microchemical Journal, 2020, 157: 104877

23. Thushari I, Babel S. Sustainable utilization of waste palm oil and sulfonated carbon catalyst derived from coconut meal residue for biodiesel production. Bioresource Technology, 2018, 248: 199–203
24. Liu T, Li Z, Li W, Shi C, Wang Y. Preparation and characterization of biomass carbon-based solid acid catalyst for the esterification of oleic acid with methanol. Bioresource Technology, 2013, 133: 618–621
25. Rafiee E, Mirnezami F. Temperature regulated Brønsted acidic ionic liquid-catalyze esterification of oleic acid for biodiesel application. Journal of Molecular Structure, 2017, 1130: 296–302
26. Peixoto A F, Soliman M M A, Pinto T V, Silva S M, Costa P, Alegria E C B A, Freire C. Highly active organosulfonic aryl-silica nanoparticles as efficient catalysts for biomass derived biodiesel and fuel additives. Biomass and Bioenergy, 2021, 145: 105936
27. Zhang P, Wu H, Fan M, Sun W, Jiang P, Dong Y. Direct and postsynthesis of tin-incorporated SBA-15 functionalized with sulfonic acid for efficient biodiesel production. Fuel, 2019, 235: 426–432
28. Kasinathan P, Lang C, Gaigneaux E M, Jonas A M, Fernandes A E. Influence of site pairing in hydrophobic silica-supported sulfonic acid bifunctional catalysts. Langmuir, 2020, 36(46): 13743–13751
29. Viscardi R, Barbarossa V, Maggi R, Pancrazzi F. Effect of acidic MCM-41 mesoporous silica functionalized with sulfonic acid groups catalyst in conversion of methanol to dimethyl ether. Energy Reports, 2020, 6: 49–55
30. Tai Z, Isaacs M A, Parlett C M A, Lee A F, Wilson K. High activity magnetic core-mesoporous shell sulfonic acid silica nanoparticles for carboxylic acid esterification. Catalysis Communications, 2017, 92: 56–60
31. Usai E M, Sini M F, Meloni D, Solinas V, Salis A. Sulfonic acid-functionalized mesoporous silicas: microcalorimetric characterization and catalytic performance toward biodiesel synthesis. Microporous and Mesoporous Materials, 2013, 179: 54–62
32. Tran T T V, Obpirompoo M, Kongparakul S, Karnjanakom S, Reubroycharoen P, Guan G, Chanlek N, Samart C. Glycerol valorization through production of *di*-glyceryl butyl ether with sulfonic acid functionalized KIT-6 catalyst. Carbon Resources Conversion, 2020, 3: 182–189
33. Decarpigny C, Bleta R, Ponchel A, Monflier E. Oxidation of 2,5-diformfylfuran to 2,5-furandicarboxylic acid catalyzed by *Candida antarctica* lipase B immobilized in a cyclodextrin-templated mesoporous silica. The critical role of pore characteristics on the catalytic performance. Colloids and Surfaces. B, Biointerfaces, 2021, 200: 111606
34. Rahman S, Shah S, Santra C, Sen D, Sharma S, Pandey J K, Mazumder S, Chowdhury B. Controllable synthesis of niobium doped mesoporous silica materials with various morphologies and its activity for oxidative catalysis. Microporous and Mesoporous Materials, 2016, 226: 169–178
35. Patel A, Brahmkhatri V. Kinetic study of oleic acid esterification over 12-tungstophosphoric acid catalyst anchored to different mesoporous silica supports. Fuel Processing Technology, 2013, 113: 141–149
36. Wang X, Zhang Y, Luo W, Elzatahry A A, Cheng X, Alghamdi A, Abdullah A M, Deng Y, Zhao D. Synthesis of ordered mesoporous silica with tunable morphologies and pore sizes via a nonpolar solvent-assisted Stöber method. Chemistry of Materials, 2016, 28 (7): 2356–2362
37. Ballistreri F P, Tomaselli G A, Toscano R M. Selective and mild oxidation of thiols to sulfonic acids by hydrogen peroxide catalyzed by methyltrioxorhenium. Tetrahedron Letters, 2008, 49(20): 3291–3293
38. Brunauer S, Deming L S, Deming W E, Teller E. On a theory of the van der Waals adsorption of gases. Journal of the American Chemical Society, 1940, 62(7): 1723–1732
39. Cano-Serrano E, Campos-Martin J M, Fierro J L G. Sulfonic acid-functionalized silica through quantitative oxidation of thiol groups. Chemical Communications, 2003, (2): 246–247
40. Kruk M, Jaroniec M, Sayari A J L. Application of large pore MCM-41 molecular sieves to improve pore size analysis using nitrogen adsorption measurements. Langmuir, 1997, 13(23): 6267–6273
41. Isaifan R J, Ntais S, Baranova E A. Particle size effect on catalytic activity of carbon-supported Pt nanoparticles for complete ethylene oxidation. Applied Catalysis A, General, 2013, 464-465: 87–94
42. Hasan Z, Jun J W, Jhung S H. Sulfonic acid-functionalized MIL-101 (Cr): an efficient catalyst for esterification of oleic acid and vapor-phase dehydration of butanol. Chemical Engineering Journal, 2015, 278: 265–271
43. Yu H, Niu S, Lu C, Li J, Yang Y. Sulfonated coal-based solid acid catalyst synthesis and esterification intensification under ultrasound irradiation. Fuel, 2017, 208: 101–110
44. Nongbe M C, Ekou T, Ekou L, Yao K B, Le Grognec E, Felpin F X. Biodiesel production from palm oil using sulfonated graphene catalyst. Renewable Energy, 2017, 106: 135–141
45. Niu S, Ning Y, Lu C, Han K, Yu H, Zhou Y. Esterification of oleic acid to produce biodiesel catalyzed by sulfonated activated carbon from bamboo. Energy Conversion and Management, 2018, 163: 59–65
46. Zhou Y, Ding H, Liu J, Parnas R S, Clearfield A, Xiao M, Meng Y, Sun L. Solid acid catalyst based on single-layer α-zirconium phosphate nanosheets for biodiesel production via esterification. Catalysts, 2018, 8(1): 1–17
47. Chen Y, Cao Y, Suo Y, Zheng G P, Guan X X, Zheng X C. Mesoporous solid acid catalysts of 12-tungstosilicic acid anchored to SBA-15: characterization and catalytic properties for esterification of oleic acid with methanol. Journal of the Taiwan Institute of Chemical Engineers, 2015, 51: 186–192
48. Yang H, Song H, Zhang H, Chen P, Zhao Z. Esterification of citric acid with *n*-butanol over zirconium sulfate supported on molecular sieves. Journal of Molecular Catalysis A Chemical, 2014, 381: 54–60